Neuron, Vol. 17, 607–615, October, 1996, Copyright ©1996 by Cell Press

GFAP Is Necessary for the Integrity of CNS White Matter Architecture and Long-Term Maintenance of Myelination

Wolfgang Liedtke,*# Winfried Edelmann,†# Phyllis L. Bieri,‡ Fung-Chow Chiu,§ Nicholas J. Cowan,‖ Raju Kucherlapati,† and Cedric S. Raine*‡§
*Department of Pathology/Division of Neuropathology
†Department of Molecular Genetics
‡Department of Neuroscience
§Department of Neurology
Albert Einstein College of Medicine
Bronx, New York 10461
‖Department of Biochemistry
New York University
New York, New York 10016

Summary

To investigate the structural role of glial fibrillary acidic protein (GFAP) in vivo, mice carrying a null mutation in GFAP were generated. In 7/14 mutant animals older than 18 months of age, hydrocephalus associated with white matter loss was detected. Mutant mice displayed abnormal myelination including the presence of actively myelinating oligodendrocytes in adults, nonmyelinated axons in optic nerve, and reduced myelin thickness in spinal cord. White matter was poorly vascularized and the blood–brain barrier was structurally and functionally impaired. Astrocytic structure and function were abnormal, consisting of shortened astrocytic cell processes, decreased septation of white matter, and increased CNS extracellular space. Thus, GFAP expression is essential for normal white matter architecture and blood–brain barrier integrity, and its absence leads to late-onset CNS dysmyelination.

Introduction

Classically, glial cells have been viewed as providers of physical and trophic support for neurons (Virchow, 1846; Kandel, 1991). The investigation of interactions between neurons and glia has long been a major focus in neuroscience, while interactions between glial cell types have received less attention. Astrocytes have been shown to be instrumental in migration, positioning, and maintenance of a functional environment for neurons (Rakic, 1981; Privat et al., 1995). Little is known about the interaction of the two major glial cell types in the CNS, i.e., astrocytes and oligodendrocytes, in vivo.

Intermediate filaments (IFs) form a group of cytoskeletal proteins believed to play a role in the mechanical strength and shape of cells and their processes (reviewed by Fuchs and Weber, 1994 and by Lazarides, 1980). In astrocytes, the major IF is glial fibrillary acidic protein (GFAP), first described in 1971 (Eng et al., 1971). Glial scarring, a sequela of a number of degenerative conditions in which up-regulation of GFAP occurs, has prompted much research aimed at the down-regulation of GFAP expression (reviewed by Eng and Ghirnikar, 1994). Studies of astrocyte–neuron interactions in vitro have shown that astrocytes rendered devoid of GFAP by an antisense GFAP RNA failed to form processes in coculture with neurons (Weinstein et al., 1991; Yu et al., 1991, 1993). More recently, GFAP$^{-/-}$ mice were reported to lack gross neurologic, behavioral, or structural CNS abnormalities (Gomi et al., 1995; Pekny et al., 1995; Shibuki et al., 1996).

The objective of the present study was to define a structural and functional phenotype for GFAP$^{-/-}$ mice to elucidate the role of GFAP in vivo. We constructed such mice and focused our studies on optic nerve and spinal cord white matter. One unexpected outcome of the work was the demonstration that GFAP is necessary for the long-term maintenance of normal CNS myelination. This novel phenotype is characterized by ongoing myelination in the adult CNS, alterations in the blood–brain barrier (BBB), disorganization of white matter architecture and vascularization, and hydrocephalus in older mice associated with loss of white matter.

Results

Generation of GFAP-Deficient Mice

The targeting vector designed pGNTK contained the PGKneo cassette inserted into the SalI site within exon 1 of the GFAP gene. This modification results in a stop codon at position 44 of the novel open reading frame. The linearized targeting vector was electroporated into E14-1 embryonic stem cells. One colony (G0906) with the desired modification was identified and verified by Southern blot. Cells from this line were injected into C57BL/6-derived blastocysts. Chimeric animals transmitted the modification through their germline.

GFAP-Deficient Mice Are Viable

F1 animals, which are heterozygous for this mutation, were interbred and their offspring genotyped by Southern blotting. Animals heterozygous and homozygous for this mutation developed normally. The mutation is transmitted in a Mendelian fashion. Western blot analysis of protein extracts from GFAP$^{-/-}$ animals demonstrated the absence of GFAP.

Gross Neuropathology, Hydrocephalus, and Evidence for Altered Myelination in GFAP$^{-/-}$ Mice

The CNS of mutant mice displayed a softened consistency, which made handling artifacts more likely.

Hydrocephalus ex-vacuo was detected in 7/14 mice between 18 and 24 months of age (Figures 1a–1d). Affected animals were neurologically normal, making an obstruction in cerebrospinal fluid circulation an unlikely cause for the hydrocephalus. Histological examination of the hydrocephalic CNS and meninges revealed no signs of ependymal erosion, inflammation, or subarachnoid hemorrhage. The Sylvian aqueduct and the central

# These two authors contributed equally to this study.

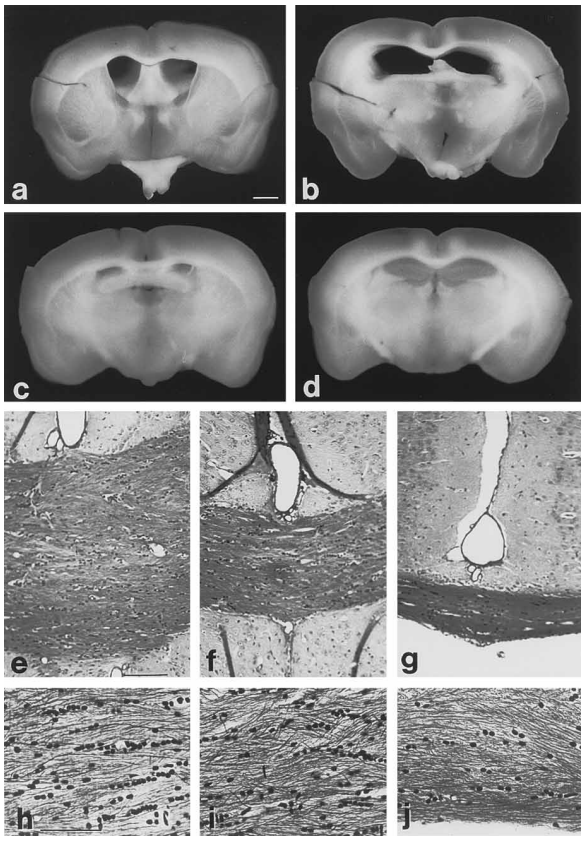

Figure 1. Hydocephalus, Associated with CNS White Matter Loss, Is Present in Older GFAP$^{-/-}$ Mice

(a) and (b) Coronal sections at the level of the optic chiasm are shown from two GFAP$^{-/-}$ mice older than 18 months of age. The degree of hydrocephaly depicted here is the minimum (a) and average (b) encountered in these mice. Scale bar, 2.5 mm.

(c) and (d) Coronal sections of brain from two wild-type littermates show the maximum (a) and average (b) amount of ventricular enlargement encountered in control mice older than 18 months of age.

(e) The corpus callosum from a wild-type mouse older than 18 months of age shows the normal thickness. Luxol fast blue; paraffin section. Original magnification, ×130. Scale bar, 100 μm.

(f) The corpus callosum from an age-matched GFAP$^{-/-}$ mouse without ventricular enlargement is reduced ~50% in thickness. Original magnification, ×130.

(g) The corpus callosum from an age-matched GFAP$^{-/-}$ mouse with hydrocephalus is severely reduced in thickness. Original magnification, ×130.

(h) Corpus callosum as in (e), stained by a Bodian axon stain, illustrates regular axon density. Original magnification, ×350. Scale bar, 50 μm.

(i) Corpus callosum as in (f), Bodian, axon density as compared to (h) slightly compacted. Original magnification, ×350.

(j) Corpus callosum as in (g), Bodian, axon density as compared to (h) slightly compacted. Original magnification, ×350.

canal were of regular appearance. Of 12 wild-type littermate controls older than 18 months of age, none showed hydrocephalus. The brains of 14 GFAP$^{-/-}$ mice and 12 controls were sectioned at the level of the optic chiasm, and CNS myelin was assessed by Luxol fast blue staining (Figures 1e–1g). The mutant animals had decreased levels of myelin. Corpus callosum thickness served as a surrogate marker for the amount of myelinated white matter. The corpus callosum was significantly thinner in hydrocephalic as well as nonhydrocephalic GFAP$^{-/-}$ mice (hydrocephalic GFAP$^{-/-}$: $p < 0.0001$, $n = 7$; nonhydrocephalic GFAP$^{-/-}$: $p = 0.0006$, $n = 5$; *t* test; wild type, $n = 9$). Axon density in the thinned corpora callosa was not decreased, as revealed by Bodian staining (Figures 1h–1j).

The finding of hydrocephalus and associated loss of white matter prompted further investigation of myelin and oligodendrocyte pathology in older mice. Oligodendrocytes actively engaged in myelination, evidenced by their clear association with myelin sheaths via prominent cytoplasmic processes (never a feature of the normal adult CNS [Raine, 1991]), were readily detectable by light microscopy in 1 μm epoxy sections (Figures 2a and 2b). Further indications of oligodendroglial immaturity were also present in the form of oligodendroglial hyperplasia, cells with irregular nuclei and an increased amount of cytoplasm, suggestive of intense biosynthetic activity (Figure 2c). Cytoplasmic processes from oligodendrocytes frequently contacted myelin sheaths of thinly myelinated fibers. These findings of oligodendrocyte pathology in the CNS of GFAP$^{-/-}$ mice were most easily detected in mice older than 1 year and were not encountered before 6 months of age or in wild-type littermates. Ultrastructural findings (Figures 2d and 2e) of large oligodendrocytes with abundant cytoplasm, cytoplasmic extensions, and processes in close proximity to myelin sheaths, similar to appearances seen during myelination (Raine, 1991), confirmed the light microscopic results. In normal rodents, all axons in the optic nerve are myelinated (Vaughn and Peters, 1967). In contrast, optic nerves of GFAP$^{-/-}$ mice showed scattered nonmyelinated axons (Figure 2e). Wild-type optic nerves failed to reveal any nonmyelinated axons. In the anterior column of the spinal cord, morphometric analysis of myelinated axons (see Experimental Procedures) revealed a statistically significant thinning of myelin sheaths in GFAP$^{-/-}$ mice ($p = 0.009$, *t* test). The mean axonal diameter did not differ between groups. Nonmyelinated axons were more numerous in the spinal cords and optic nerves of GFAP$^{-/-}$ mice; there were 0 nonmyelinated axons of 985 axons counted in wild-type spinal cord ($n = 4$) versus 52 unmyelinated of 920 axons in the matched GFAP$^{-/-}$ animals ($n = 4$). In optic nerve, wild-type mice did not show nonmyelinated axons in a total of 2615 axons counted versus 30 nonmyelinated axons of 2465 axons in GFAP$^{-/-}$ mice. Measurement of myelin thickness in optic nerves revealed no differences between wild-type and mutant mice. As with light microscopy, ultrastructural findings of altered myelination tended to be more pronounced in older mutant mice. No oligodendroglial staining for the developmental IF nestin (Gallo and Armstrong, 1995) or the oligodendrocyte marker A2B5 (Abney et al., 1983) was observed.

The BBB Is Morphologically and Functionally Altered in GFAP$^{-/-}$ Mice

In mutant mice, the BBB comprised a single layer of astrocytic endfeet with very few IFs in the spinal cord and some IFs in the optic nerve (Figures 2f and 2g). Permeability studies with ^{125}I-labeled albumin revealed increased permeability in the lumbar spinal cord of

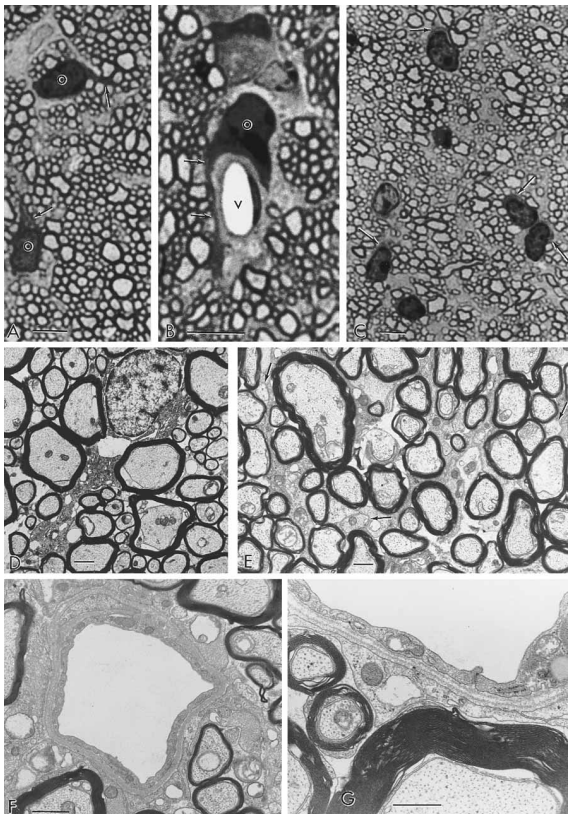

Figure 2. CNS Myelination and BBB Are Abnormal in Adult GFAP$^{-/-}$ Mice

(a) Two oligodendrocytes (o) are seen in the optic nerve of a 14-month-old GFAP$^{-/-}$ mouse to extend thick cytoplasmic processes (arrows) to myelinated nerve fibers. Such appearances are not seen in the normal adult CNS. Toluidine blue stained 1 μm epoxy section. Original magnification, ×1120. Scale bar, 10 μm.

(b) An oligodendrocyte (o) of a 14-month-old mouse is shown engaged in myelination in the optic nerve. It is attached to a new fiber by a long process (arrows). The cell body is wrapped around a small blood vessel, lumen at (v). Original magnification, ×1920. Scale bar, 10 μm. Similar preparation to (a).

(c) Numerous oligodendrocytes are seen in the optic nerve of a 14-month-old GFAP$^{-/-}$ mouse. Note the dense irregularly shaped nuclei and the prominent rim of cytoplasm around each of them. Similar preparation to A. Original magnification, ×800. Scale bar, 10 μm.

(d) An electron micrograph from the spinal cord white matter from an 8-month-old GFAP$^{-/-}$ mouse depicts an oligodendrocyte that extends a long process toward the lower left corner. The vacuole in the cytoplasm immediately beneath the nucleus is a preparation artifact. Original magnification, ×6700. Scale bar, 1 μm.

(e) An electron micrograph of optic nerve white matter from a 6-month-old GFAP$^{-/-}$ mouse reveals three nonmyelinated nerve fibres (arrows). The nonmyelinated axon in the center is a cross section of a nodal axon with a paranodal loop of oligodendrocyte cytoplasm below. Original magnification, ×6000. Scale bar, 1 μm.

(f) An electron micrograph of a normal blood vessel in the spinal cord is shown from a wild-type littermate control mouse. Note multiple layers of astroglial cell processes around the endothelium rich in glial fibrils. Original magnification, ×12000. Scale bar, 1 μm.

(g) An electron micrograph of the BBB from a GFAP$^{-/-}$ spinal cord shows the endothelium of a blood vessel surrounded by two layers of basal lamina and a single layer of perivascular astroglial cell processes, which contains an occasional IF only. Note the loose contact between adjacent astroglial cells at the upper left and the gap junction at center right. The extracellular space is increased. Original magnification, ×30.000. Scale bar, 0.5 μm.

GFAP$^{-/-}$ animals one year or older ($p = 0.0037$, Mann–Whitney U test). In the brain, the results were more variable.

White Matter Is Poorly Vascularized in GFAP$^{-/-}$ Mice

Examination of 1 μm sections and electron microscopy (EM) indicated that fewer vessels were present in the white matter of mutant animals. Endothelial cells in optic nerves of 4-month-old mice were stained for the endothelial cell marker glucose transporter 1, and counted (see Experimental Procedures and Figures 3a and 3b). The number of vessels in optic nerve was statistically significantly decreased in GFAP$^{-/-}$ animals ($p < 0.0001$, Mann–Whitney U test). Large-caliber vessels were rare in mutant mice but readily detectable in wild-type littermates, and the center of the optic nerve was less vascularized in GFAP$^{-/-}$ animals. In the spinal cord, it was difficult to obtain clear-cut morphometric data because of penetrating vessels to the gray matter. However, a poorer vascularization of GFAP$^{-/-}$ white matter was also apparent in the spinal cord.

White Matter Is Disorganized in GFAP$^{-/-}$ Mice

Optic Nerve

As seen in 1 μm sections, astrocytic processes separating optic nerve by means of septa were barely visible in GFAP$^{-/-}$ mice, in contrast to wild-type littermate controls (data not shown). Immunocytochemistry for vimentin in the mutant, and for vimentin and GFAP in the wild-type littermates, supported this observation (Figures 3c–3f). In the wild-type littermates, the regular astrocytic network organizing the optic nerve was formed by astrocytic processes positive for vimentin and GFAP. In GFAP$^{-/-}$ mice, this network appeared less well organized and was positive for vimentin only (Figure 3f), but Western blotting for vimentin showed no upregulation in mutant animals (data not shown). Other astrocyte markers such as S100β and glutathione S-transferase confirmed the vimentin staining pattern (data not shown). At the EM level, IF bundles were present in both types of animals (Figures 3g and 3h). By immuno-EM, the IF consisted of GFAP and vimentin in the wild-type littermates and vimentin only in the mutant (data not shown).

Spinal Cord

As observed in 1 μm sections, astrocytic processes formed septa in wild-type littermates and failed to do so in GFAP$^{-/-}$ mice (Figures 4a and 4b). Immunohistochemistry confirmed the absence of GFAP in the mutant and its presence in the wild-type (Figures 4c and 4d). Immunostaining revealed vimentin in astrocytic processes of wild-type mice and in cell bodies of GFAP$^{-/-}$ astrocytes (Figures 4e and 4f). Staining for S100β and glutathione S-transferase confirmed the astrocyte morphology (data not shown). These findings were extended ultrastructurally whereby wild-type astrocytes had abundant IFs in their processes (Figure 5a). These processes were prominent and in close contact with myelin sheaths, unmyelinated axons, and glial cell bodies. Immuno-EM demonstrated that these processes contained vimentin and GFAP (Figures 5b and 5c). In

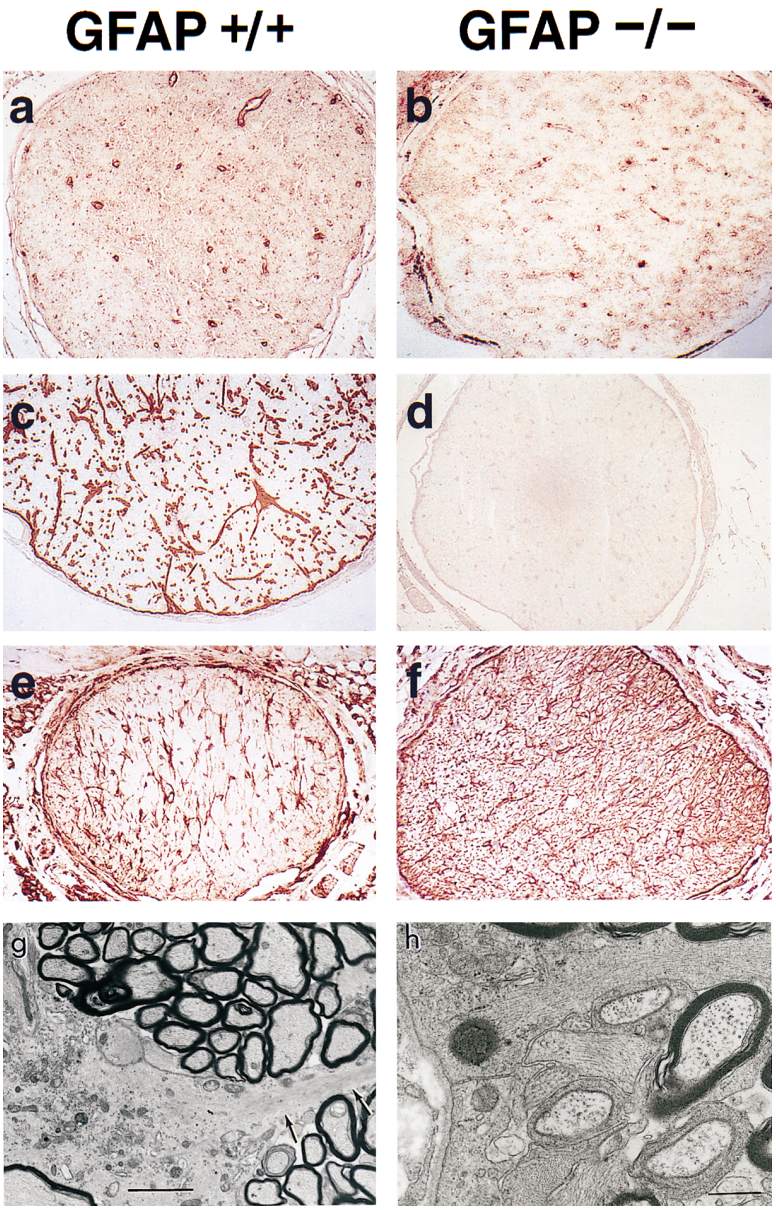

Figure 3. Optic Nerve White Matter Vascularization and Architecture Are Abnormal in GFAP$^{-/-}$ Mice

(a) The optic nerve of a wild-type littermate control mouse is immunostained with anti-glucose transporter 1, an endothelial cell marker. Note the even distribution of labeled blood vessels throughout the nerve. Original magnification, ×170.

(b) Similar staining performed on a GFAP$^{-/-}$ optic nerve. Note the paucity of vascularization evidenced by the small amount of reactivity to glucose transporter 1. Original magnification, ×170.

(c) Wild-type littermate control mouse; 1 μm epoxy section immunoreacted for GFAP (monoclonal antibody). Note the extensive arborization of astrocytic processes and the intense reactivity for GFAP along the glia limitans. Original magnification, ×220.

(d) A corresponding stain for GFAP in a GFAP$^{-/-}$ animal confirms the absence of GFAP. Original magnification, ×160.

(e) A formalin-fixed paraffin-embedded section from the optic nerve of a wild-type littermate control mouse is specifically stained for vimentin. Note the astrocytic scaffold throughout the nerve. Original magnification, ×160.

(f) A corresponding section from a GFAP$^{-/-}$ mouse reacted for vimentin. Note the slightly increased immunoreactivity and the decreased organization of the optic nerve by astroglial processes. Original magnification, ×160.

(g) An electron micrograph of an area of subpial optic nerve is shown from a wild-type littermate control mouse. Note the subpial astrocyte extending a long process rich in glial filaments (arrows) into the white matter. Original magnification, ×6800. Scale bar, 2 μm.

(h) Electron micrograph of processes from subpial optic nerve GFAP$^{-/-}$ astrocytes that contain abundant IF. In the center, note the unusual occurrence of several paranodal axons surrounded by a layer of oligodendrocyte cytoplasm. Original magnification, ×10.000. Scale bar, 1 μm.

animals of all ages, rudimentary processes from GFAP$^{-/-}$ astrocytes appeared short and club-like (Figures 5d–5f). Intimate contact of these extensions with other white matter structures did not occur. The extracellular space was appreciably increased. Nodes of Ranvier displayed a different morphology in the mutant (Figure 5f). In many cases, an astrocytic cell body with its short processes was directly associated with a nodal axolemma. This phenomenon is not seen in normal wild-type animals (Raine, 1984). GFAP$^{-/-}$ astrocytes contained an occasional IF. Desmosomes and gap junctions were present in both types of animals (Figures 5a, 5d, and 5e).

Electrophysiological Findings: Visual Evoked Potentials Are Normal in GFAP$^{-/-}$ Mice

Visual evoked potentials (VEPs) were recorded from visual cortex. Onset of current flow was not significantly different between groups, nor was the magnitude or duration of total intracortical current flow (data not shown).

Search for Compensatory IF Expression and Markers for Immature Oligodendroglia Are Unremarkable: Additional Observations

1 μm sections of cerebrum, cerebellum, and brainstem revealed no differences between groups. Except for the presence or absence of GFAP, the same was true with immunohistochemistry.

No staining was obtained for other IFs and the developmental antigen brain-lipid-binding protein (Fuchs and Weber, 1994; Feng et al., 1994). Cortical Nissl staining revealed no differences in cortical architecture between the two types of animals. Western blotting of optic nerve proteins for the IF nestin was negative in both groups.

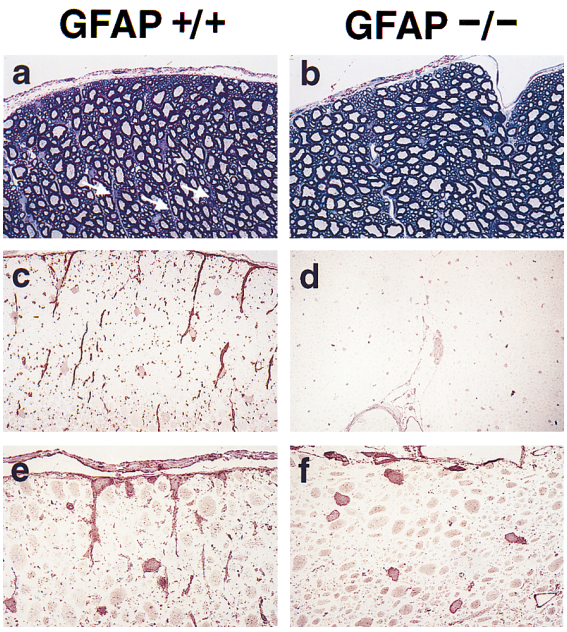

Figure 4. Spinal Cord White Matter Architecture Is Abnormal in GFAP$^{-/-}$ Mice

(a) A toluidine blue–stained 1 μm epoxy section shows radiating astrocytic processes (arrows) in an anterior column of a wild-type littermate control mouse. Original magnification, ×400

(b) A similar section to (a), taken from a matched GFAP$^{-/-}$ mouse. Note the lack of radiating astroglial cell processes. Original magnification, ×400.

(c) A 1 μm epoxy section from a wild-type littermate control mouse is specifically stained for GFAP (monoclonal antibody). This demonstrates that the radial processes express GFAP. Original magnification, ×400.

(d) A corresponding section from a GFAP$^{-/-}$ mouse confirms the lack of GFAP immunoreactivity. Original magnification, ×400.

(e) A 1 μm epoxy section of anterior column from a wild-type littermate control mouse is specifically stained for vimentin (monoclonal antibody). Note the presence of vimentin in the radiating and transversely sectioned astroglial cell processes and along the glia limitans. Axons in cross section show faint cross-reactivity. Myelin sheaths are seen as negative images. Original magnification, ×675.

(f) Corresponding section from a matched GFAP$^{-/-}$ mouse also immunoreacted for vimentin. Note the positively stained astroglial cell bodies essentially devoid of cell processes and the patchy staining along the glia limitans. Axons show the same degree of cross-reactivity as in (e). Original magnification, ×675.

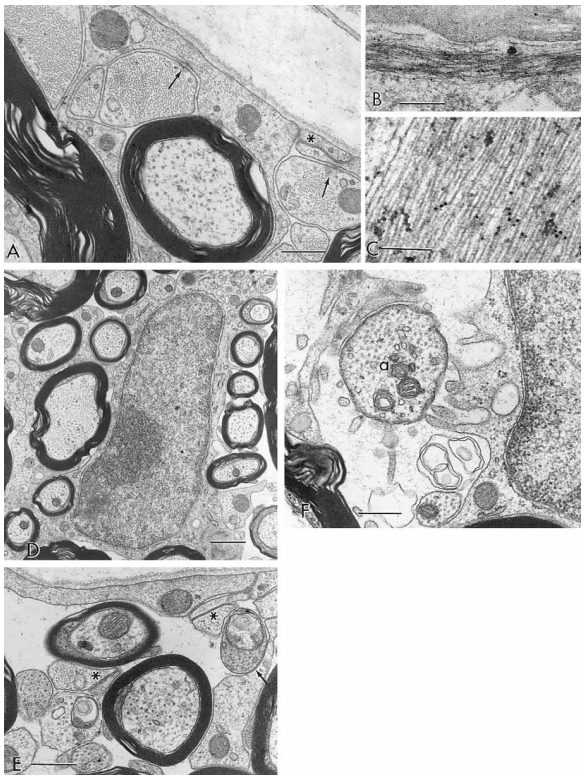

Figure 5. Ultrastructure of Spinal Cord

(a) Subpial spinal cord white matter from a wild-type mouse shows bundles of glial filaments within astrocytic processes. Note the desmosomes (arrows), gap junction (asterisk), and basal lamina along the glia limitans. There is an absence of an extensive extracellular space. Original magnification, ×28.000. Scale bar, 0.5 μm.

(b) Immunogold labeling for GFAP in spinal cord white matter of a wild-type littermate control mouse. Note the gold particles decorating the glial filaments. Original magnification, ×30.000. Scale bar, 0.5 μm.

(c) Immunogold labeling for vimentin; wild-type spinal cord. Note the gold particles overlying the astroglial filaments. Original magnification, ×60.000. Scale bar, 0.25 μm.

(d) An astrocyte within the spinal cord white matter from a GFAP$^{-/-}$ mouse extends short cell processes between the myelinated nerve fibers to the right. Note the long gap junction on the cell surface toward the lower left. Original magnification, ×11.000. Scale bar, 1 μm.

(e) Subpial white matter from a GFAP$^{-/-}$ mouse reveals a thin layer of astrocytic processes along the glia limitans as well as an extensive extracellular space. Gap junctions are seen at the asterisk. Note the relative paucity of glial filaments. Original magnification, ×27.000. Scale bar, 0.5 μm.

(f) A transversally sectioned axon (a) at a node of Ranvier is flanked by villus-like extensions from an astrocyte cell body (nucleus, right). Such close proximity between astrocytic processes at a node of Ranvier and the cell of origin is most unusual in normal animals. Original magnification, ×30.000. Scale bar, 0.5 μm.

Discussion

In the present investigation, we report a novel structural phenotype for GFAP-deficient mice. Older GFAP$^{-/-}$ mice had white matter loss, and hydrocephalus was present in 50% of cases. In addition, other abnormalities in myelination could be detected. Oligodendrocytes were seen to be engaged in active myelination in adult GFAP$^{-/-}$ mice. This appeared to be a late-onset defect of myelination homeostasis in GFAP$^{-/-}$ animals and was not seen in animals younger than 6 months of age. Myelination in the optic nerve and spinal cord was perturbed, with nonmyelinated axons present in the optic nerve, and thinned myelin and increased numbers of nonmyelinated axons present in the spinal cord anterior column. The astrocytic scaffold was disturbed throughout the white matter, and the BBB was more permeable in the GFAP$^{-/-}$ mouse. Altered myelination in GFAP$^{-/-}$ mice suggests a novel link (direct or secondary consequence) between astrocytic function and the maintenance of myelination.

A late-onset imbalance in myelin homeostasis was

suggested by the following pattern. Hydrocephalus became obvious in animals older than 18 months of age, morphologic evidence of oligodendrocyte immaturity was detectable in animals older than 12 months of age, and ultrastructural alterations in myelination and oligodendrocyte morphology were visualized in mice older than 6–8 months. We found a number of possible contributing factors in this defective long-term maintenance of myelination. EM demonstrated short club-like processes of astrocytes and increased extracellular space in GFAP$^{-/-}$ animals. This might lead to reduced contact between astrocytes and oligodendrocytes, and between astrocytes and myelin sheaths. The paucity of white matter vascularization might lead to an impaired supply of nutrients for myelin and myelinating cells. Increased permeability of the BBB may also underlie the entry of circulating factors, e.g., complement (Wren and Noble, 1989), that may be detrimental for oligodendrocytes and myelin sheaths. Thus, we cannot rule out that myelination abnormalities and hydrocephalus might be secondary consequences of a lack of GFAP expression in mutant mice. Although the observed hydrocephalus and thinning of the corpus callosum in GFAP$^{-/-}$ mice clearly segregated with the targeted allele, the genetic background of our mice might be regarded as a modifying cofactor.

Abnormalities in optic nerve myelination were present in the form of nonmyelinated axons and myelinating oligodendrocytes. The presence of these changes suggests that expression of vimentin in optic nerve astrocyte processes was unable to compensate entirely for the lack of GFAP. Compensation at the functional level appeared to be complete, since VEPs were normal.

Morphologic and functional alterations of the BBB in GFAP$^{-/-}$ animals demonstrate the importance of GFAP in the integrity of this structure. A statistically significant difference for ^{125}I-albumin permeability was recorded only in lumbar spinal cord of mice older than 12 months of age because of the known gradient of GFAP expression in spinal cord and because of the increased GFAP expression with age (Goss et al., 1991; Landry et al., 1990). Results in the brain were more variable because of regions of increased BBB permeability.

The reduced vascularization and altered vascular architecture in GFAP$^{-/-}$ white matter may reflect a malfunction of astrocytic induction mechanisms for vascularization. The observed phenotype in mutant mice might be regarded as a developmental abnormality where vessels are not as efficiently induced and guided by astrocytes and by their precursors that are devoid of GFAP (Janzer and Raff, 1987). As discussed above, poorer white matter vascularization might be linked to altered myelination. Beyond that, no other consequences were apparent.

In the first report on GFAP$^{-/-}$ mice, it was emphasized that these mice lacked gross neurologic or behavioral abnormalities and that they were susceptible to scrapie (Gomi et al., 1995). In contrast, structural aberrations and an altered BBB were readily apparent in the present study. One major reason for this discrepancy may lie in the CNS regions studied (at least six levels of spinal cord and two regions of optic nerves in our study), differences in methodology (toluidine blue–stained semithin sections as initial screening), and different age groups (2 months to 2 years of age) examined.

In another study, GFAP$^{-/-}$ animals were investigated after cerebral stab wound. They reportedly showed a lack of structural abnormalities, GFAP$^{-/-}$ astrocytes devoid of IF, and a regular BBB function as examined by Evans blue injection (Pekny et al., 1995). Since Evans blue staining is less sensitive than ^{125}I-albumin, and since spinal cord was not included in the investigation of the BBB, the different results are not surprising. While we agree with Pekny et al. (1995) on the absence of IF bundles in GFAP$^{-/-}$ spinal cord astrocytes, these cells are, according to our data, not totally devoid of IF.

In a third study, deficient cerebellar long-term depression and impaired eyeblink conditioning were reported in GFAP$^{-/-}$ mice, indicating GFAP to be necessary for interactions between Bergmann glia and Purkinje cells (Shibuki et al., 1996). Structural abnormalities or mechanistic insights into the observed phenomena were not provided. The former might have been expected in view of the results of previous work in vitro, where astrocytes transfected with a GFAP antisense RNA did not extend processes when cocultured with neurons (Weinstein et al., 1991).

In a recent study, it was reported that altered hippocampal long-term potentiation occurred in GFAP$^{-/-}$ mice (McCall et al., 1996). Optic nerve GFAP$^{-/-}$ astrocytes were detected to contain IF bundles. Our observations are in line with this, and we have gone on to show that these filaments are vimentin.

The present study documents a novel role for GFAP in the long-term maintenance of myelination in vivo, indicating possible cross-talk between astrocytes and oligodendrocytes or secondary consequences of a lack of GFAP expression. For astrocytes to perform properly in this scenario, and for CNS myelination to retain structural integrity, normal expression of GFAP appears to be mandatory.

Astroglia–oligodendroglia interactions in vivo (Bunge et al., 1961; Bunge and Glass, 1965) were found to be significant in the jimpy mouse (Skoff, 1976). In the latter study, abnormal branching of astrocytes and sequestration of axons by astrocytes prior to myelination were reported to be the likely causes of abnormal oligodendroglial development. It was later suggested by in vitro studies that normal astrocytes produce soluble factors that promote the normal functioning of otherwise defective jimpy oligodendrocytes (Bartlett et al., 1988). In another study, transgenic mice expressing a polyoma virus antigen in astrocytes were reported to show CNS dysmyelination (Baron-van Evercooren et al., 1992). The pathogenesis in the latter two types of mutant mice is suggestive of altered glia–glia interactions. In contrast with the present observations, the dysmyelination was more striking and manifested as a disorder of early postnatal development. Investigations on remyelination after application of gliotoxins have suggested that astrocytes facilitate remyelination (Blakemore and Franklin, 1991). Astroglia–oligodendroglia interactions in vitro have demonstrated that astrocyte-produced platelet-derived growth factor (PDGF) is important for oligodendroglial development (Richardson et al., 1988; Noble et al., 1988; Raff et al., 1988). Basic fibroblast growth factor modulated these PDGF effects (McKinnon et al., 1990; Boegler

et al., 1990). A novel leukemia-inhibitory factor–related cytokine has been reported to act as a regulator of later stages of oligodendroblast/oligodendrocyte development and survival (Gard et al., 1995).

Taken together, GFAP$^{-/-}$ mice display a structural phenotype with topographical variation in IF expression, disrupted white matter architecture, and late-onset disturbances of CNS myelination.

Experimental Procedures

Construction of the pGNTK Targeting Vector

A 2.0 kb EcoRI–SalI fragment spanning the GFAP promoter region was used to screen a Charron 35 129/Ola mouse genomic l-phage library (Balcarek and Cowan, 1985). A 3.4 kb BglII fragment spanning the GFAP promoter region , exon 1, exon 2, and part of exon 3 was subcloned into the BamHI site of pcDNAII (Invitrogen, La Jolla, CA). A MC1tk SalI–XhoI fragment was blunt ended and cloned into the single HindIII site treated with Klenow enzyme. A SalI–XhoI fragment containing the PGKneo cassette was cloned in the reverse transcriptional orientation into the SalI site in exon 1. The stop codon at position 44 of the resulting new open reading frame was identified by sequencing.

Electroporation of Embryonic Stem Cells

The targeting vector pGNTK was linearized at the unique NotI site, electroporated into E14-1 embryonic stem cells, and selected with G418 and ganciclovir as previously described (Handyside et al., 1989; Sirotkin et al., 1995). Doubly resistant colonies were screened by a PCR-based approach. One positive cell line (G0609) was identified, and the correct targeting event was verified by Southern blot analysis.

Generation of GFAP-Deficient Mice

We injected 8–12 stem cells derived from the positive cell line G0609 into C57BL/6 blastocysts. Male chimeric mice were bred to C57BL/6 females, and several animals transmitted the mutation through their germline. F1 heterozygotes were interbred to obtain GFAP-deficient animals. The animals for this study were of a mixed 129/Ola × C57BL/6 genetic background and stemmed from F2 and F3 generations.

Clinical Assessment of Mice

At various timepoints during the lifetime of the animals and before sacrifice, mice were clinically and neurologically examined as described for assessment of mice with experimental allergic encephalomyelitis (Moore et al., 1987). Unremarkable findings in all age groups examined were confirmed independently by different observers.

Gross Neuropathology and CNS Tissue Processing

Mice between 2 months and 2 years of age were studied.

Mice were perfused transcardially with either fixative (10% formalin or 2.5% glutaraldehyde) or phosphate-buffered saline (PBS). Formalin-perfused CNS was embedded in paraffin; glutaraldehyde-fixed CNS was postfixed in 1% osmium tetroxide, dehydrated, and embedded in epon. PBS-perfused CNS was snap-frozen and embedded in OCT or processed for Western blotting in 8 M urea. To evaluate hydrocephalus, formalin-fixed brains were sectioned coronally at the level of the optic chiasm.

Histopathology

CNS of mice perfused with glutaraldehyde was sampled at ten different levels and 1 μm semithin sections were stained with toluidine blue. Formalin-perfused paraffin-embedded CNS tissue was used for hematoxylin–eosin, Luxol fast blue, Nissl, and Bodian stains.

Immunohistochemistry

Immunohistochemistry was performed as described previously (Wu and Raine, 1992). In brief, the sections were incubated with primary antibody and reacted using the vectastain ABC kit (Vector, Burlingame, CA). Formalin-fixed tissue was used for IF stains, other astroglial markers, and glucose transporter 1, an endothelial cell marker. The following antibodies were used: anti-GFAP polyclonal rabbit antibody (Biogenex, San Ramon, CA); monoclonal mouse IgG antibody 18-0021 (Zymed, San Francisco, CA); anti-vimentin monoclonal mouse IgM antibody MAB 1681 (Chemicon International, Temecula, CA); anti-S100β polyclonal rabbit antibody (Dako, Carpinteria, CA); monoclonal mouse IgG antibody SH-B1 (Sigma, St. Louis, MO); anti-glutathione S-transferase polyclonal rabbit antibody (a gift from Dr. W. Cammer, Albert Einstein College of Medicine); anti-glucose transporter 1 polyclonal rabbit antibody (a gift from Dr. P. Davies, Albert Einstein College of Medicine); anti-nestin polyclonal rabbit antibody (a gift from Dr. R. McKay, NIH, Bethesda, MD); anti-nestin monoclonal antibody Rat 401 (Developmental Studies Hybridoma Bank, Iowa City, IA); anti-desmin polyclonal rabbit antibody; anti-α internexin polyclonal rabbit antibody; anti-keratin monoclonal mouse IgG antibody; anti-peripherin polyclonal rabbit antibody (the last four antibodies were from Chemicon International). Dilution of monoclonal antibodies ranged from 1:4 to 1:50, except for the monoclonal antibody against S100β (1:10000). Polyclonal antibodies were diluted 1:1000 to 1:2000.

Epon-embedded 1 μm sections were stained only for IF. Antibody dilutions were a factor 2 lower than those used on formalin-fixed tissue.

Frozen tissue was sectioned at 10 μm and fixed for 1 hr in a molecular biology tissue fixative (Histochoice™, Amresco, Solon, OH). These sections were used for staining with antibodies against IF, polyclonal rabbit antibody against brain-lipid-binding protein (a gift from Dr. N. Heintz, Rockefeller University, NY), and monoclonal IgM antibody A2B5 (a gift from Dr. R. Marmur, Albert Einstein College of Medicine).

EM

Thin sections of epon-embedded tissue were mounted on 200 mesh copper grids, stained with lead and uranium salts, carbon coated, and scanned in a Siemens 101.

Immune EM

This technique was performed according to previous protocols (Moore and Raine, 1988). In brief, sections were mounted on 200 mesh formvar-coated nickel grids and etched with sodium–ethoxide/ethanol (1:10) and 7.5% sodium metaperiodate, incubated with primary antibody (polyclonal GFAP antibody, diluted 1:50, and vimentin monoclonal IgM antibody, diluted 1:15), biotinylated secondary antibody, and gold particles coupled to streptavidin (Amersham, Arlington Heights, IL).

Morphometry

Ventricular enlargement in a series of 14 GFAP$^{-/-}$ mice and 12 wild-type littermate controls older than 18 months of age was determined. Two representative brains with ventricular enlargement from the group of GFAP$^{-/-}$ mice are shown in Figure 1. These were the brains with the least and an average amount of ventricular enlargement from a total of seven hydrocephalic brains from 14 mutant mice. Of the 12 control brains, one specimen illustrated in Figure 1 had the widest ventricles, one a regular appearance.

Corpus callosum thickness was measured on an enlarged micrograph of a Luxol fast blue stain taken at constant magnification.

Glucose transporter 1–stained sections were used to determine the extent of vascularization of optic nerve and spinal cord white matter. The optic nerve had been dissected 2 mm from the optic chiasm. Optic nerves were subsequently cut for skip serial 5 μm sections 100 μm apart. Ten sections spanning 1 mm of optic nerve were prepared from each sample. The same procedure was applied to segments of spinal cord tissue. Four GFAP$^{-/-}$ mice and four wild-type littermate controls, 4 months of age, were studied. Vessels were counted, and only sections where all vessels on a given cross section could be unequivocally identified (i.e., no artifacts in the tissue) were used for morphometric analysis. A mean value of vessels per cross section was calculated for each animal, and statistical analysis was performed.

EM morphometry was performed on sections of anterior column

of the cervical spinal cord (C7) and of optic nerve sectioned 2 mm from the optic chiasm. Four animals from each set were precisely matched. The animals were 6–12 months of age. Five to six electron micrographs at a magnification of 4000× were obtained from each animal and printed at a constant enlargement (×3). Spinal cord anterior column white matter was selected. On a given micrograph, all axons (nonmyelinated, internodal, and paranodal) were counted. In addition, ten axons per micrograph were randomly selected to represent the range of small and large axons. Axonal diameter and myelin thickness were determined in millimeters. In the case of oblique sectioning of an axon, the smallest diameter was taken. In the case of varied myelin thickness due to fixation, the smallest diameter was chosen. Myelin thickness as percentage of the axonal diameter was calculated as mean value per animal and subsequently used for statistical analysis. Mean axonal diameter was also calculated to control for representative choice of axons.

Immunoblotting Analysis

This procedure was performed as described previously (Chiu et al., 1989). Specifically, the following antibodies were used: anti-GFAP monoclonal antibody (clone G-A-5, Boehringer Mannheim, Indianapolis, IN) and anti-vimentin antibodies (clone Vim3B4, Boehringer-Mannheim; MAB 1681, Chemicon International, Temecula, CA). Nestin was analyzed by immunoblotting with monoclonal antibody Rat 401 (Developmental Hybridoma Studies Bank, Iowa City, IA). For optic nerves, a neurofilament blot was included as a standard (polyclonal rabbit anti-neurofilament L antibody, [Chiu et al., 1989]).

BBB Assessment with ^{125}I

This assay was performed as described previously (Goldmuntz et al., 1986). In brief, animals were intravenously injected with ^{125}I-bovine serum albumin (ICN Chemicals, Irvine, CA). Whole blood was obtained 15 hr later, and the animals were perfused. Specific activity was measured in serum, in whole spinal cord, in lumbar spinal cord, and in brain. Permeability was expressed as counts in CNS/[counts in serum × weight]. Animals younger and older than 12 months of age were measured ($n = 3$). After the first set of data, seven additional animals older than 12 months of age were examined.

Electrophysiologic Methods

VEPs were recorded and analyzed as described (Michaelson et al., 1996). In brief, these studies were performed on five GFAP$^{-/-}$ and five wild-type littermates, at age 20 weeks. VEPs were obtained using full-field stroboscopic flashes at a rate of two per second in blocks of 100 flashes. A 16-channel multicontact electrode was introduced into visual cortex, and VEPs were obtained simultaneously from multiple cortical laminae. One-dimensional current–source density (CSD) analyses of the VEP profiles were calculated as described (Nicholson and Freeman, 1975). The total rectified current was averaged for all visual hemispheres within a group, providing a grand average waveform for comparison across groups.

Statistics

Sets of data from GFAP$^{+/+}$ and GFAP$^{-/-}$ mice were analyzed by *t* test or Mann–Whitney U test, applying a statistics program (Sigmastat™, Jandel Software, San Rafael, CA).

Acknowledgments

All correspondence should be addressed to W. L.

We thank Dr. Celia F. Brosnan for her help in the experiments evaluating the BBB and helpful discussion, Dr. Yvonne Kress for advice on immunogold labeling, Dr. David Weinstein for his critical reading of the manuscript, Dr. Ronen Marmur for helpful discussion, and Everett Swanson, Howard Finch, Miriam Pakingan, Kirkland Lau, and Jorge Bermudez for skilled technical assistance. For the generous supply of antibodies, we thank the following investigators: Dr. Nathaniel Heintz and Dr. Arturo Alvarez-Buylla, Rockefeller University, NYC; Drs. Wendy Cammer, Peter Davies, and Ronen Marmur, Albert Einstein College of Medicine, Bronx, NY; and Dr. Ronald McKay, Bethesda, MD.

Supported in part by a Feodor Lynen fellowship award to W. L. from the Alexander von Humboldt Foundation, Bonn, Germany; by NSPHS grants NS 08952, NS 11920, and NS 07098; by National Multiple Sclerosis Society Grant RG 1001-I-9; and by the Human Genetics Program at the Albert Einstein College of Medicine.

The costs of publication of this article were defrayed in part by the payment of page charges. This article must therefore be hereby marked *"advertisement"* in accordance with 18 USC Section 1734 solely to indicate this fact.

Received June 12, 1996; revised August 12, 1996.

References

Abney, E.R., Williams, B.P., and Raff, M.C. (1983). Tracing the development of oligodendrocytes from precursor cells using monoclonal antibodies, fluorescence-activated cell sorting and cell culture. Dev. Biol. *100*, 166–171.

Balcarek, J.M., and Cowan, N. (1985). Structure of the mouse glial fibrillary protein gene: implications for the evolution of the intermediate filament multigene family. Nucl. Acids Res. *13*, 5527–5543.

Baron-van Evercooren, A., Jensen, N.A., Wyss, M.T., Cuzin, F., Rassoulzadegan, M., Brucher, J.M., and Baron, H. (1992). Transgenic mice expressing polyoma virus large T antigen in astrocytes develop severe dysmyelination of the central nervous system. Lab. Invest. *66*, 39–53.

Bartlett, W.P., Knapp, P.E., and Skoff, R.P. (1988). Glial conditioned medium enables jimpy oligodendrocytes to express properties of normal oligodendrocytes: production of myelin antigens and membranes. Glia *1*, 253–259.

Blakemore, W.F., and Franklin, J.M. (1991). Transplantation of glial cells into the central nervous system. Trends Neurosci. *14*, 323–327.

Boegler, O., Wren, D., Barnett, S.C., Land, H., and Noble, M. (1990). Cooperation betwen two growth factors promotes extended self-renewal and inhibits differentiation of oligodendrocytes-type-2 astrocyte (o-2A) progenitor cells. Proc. Natl. Acad. Sci. USA *87*, 6368–6372.

Bunge, R.P., and Glass, P.M. (1965). Some observations on myelin–glial relationships and on the etiology of the cerebrospinal fluid exchange lesion. Ann. NY Acad. Sci. *122*, 15–28.

Bunge, M., Bunge, R.P., and Ris, H. (1961). Ultrastructural study of remyelination in an experimental lesion in adult cat spinal cord. J. Biophys. Biochem. Cytol. *10*, 67–94.

Chiu, F.-C., Barnes, E.A., Das, K., Haley, J., Socolow, P., Macaluso, F.P., and Fant, J. (1989). Characterization of a novel 66 kD subunit of mammalian neuronal intermediate filaments. Neuron *2*, 1435–1445.

Eng, L.F., and Ghirnikar, R.S. (1994). Glial fibrillary acidic protein and astrogliosis. Brain Pathol. *4*, 229–237.

Eng, L.F., Vanderhaeghen, J.J., Bignami, A., and Gerstl, B. (1971). An acidic protein isolated from fibrous astrocytes. Brain Res. *28*, 351–354.

Feng, L., Hatten, M.E., and Heintz, N. (1994). Brain-lipid-binding protein (BLBP): a novel signaling system in the developing mammalian CNS. Neuron *12*, 895–908.

Fuchs, E., and Weber, K. (1994). Intermediate filaments: structure, dynamics, function and disease. Annu. Rev. Biochem. *63*, 345–382.

Gallo, V., and Armstrong, R.C. (1995). Developmental and growth factor–induced regulation of nestin in oligodendrocyte lineage cells. J. Neurosci. *15*, 394–406.

Gard, A.L., Burrell, M.R., Pfeiffer, S.E., Rudge, J.S., and Williams, W.C., II. (1995). Astroglial control of oligodendrocyte survival mediated by platelet derived growth factor and leukemia-inhibitory factor–like protein. Development *121*, 2187–2197.

Goldmuntz, E.A., Brosnan, C.F., and Norton, W.T. (1986). Prazosin treatment suppresses increased vascular permeability in both acute and passively transferred experimental autoimmune encephalomyelitis in the Lewis rat. J. Immunol. *137*, 3444–3450.

Gomi, H., Yokoyama, T., Fujimoto, K., Ikeda, T., Katoh, A., Itoh, T., and Itohara, S. (1995). Mice devoid of the glial fibrillary acidic protein develop normally and are susceptible to scrapie prions. Neuron *14*, 29–41.

Goss, J.R., Fich, C.E., and Morgan, D.G. (1991). Age related changes in glial fibrillary acidic protein mRNA in the mouse brain. Neurobiol. Aging *12*, 165–170.

Handyside, A.H., O'Neill, G.T., Jones, M., and Hooper, M.L. (1989). Use of BRL-conditioned medium in combination with feeder layers to isolate a diploid embryonal stem cell line. Roux's Arch. Dev. Biol. *198*, 48–55.

Janzer, R.C., and Raff, M.C. (1987). Astrocytes induce blood–brain barrier properties in endothelial cells. Nature *325*, 253–256.

Kandel, E.R. (1991). Nerve cells and behavior: glial cells. In Principles of Neural Science. E.R. Kandel, J.H. Schwartz, and T.M. Jessell, eds. (New York: Elsevier), pp. 22–24.

Landry, C.F., Ivy, G.O., and Brown, I.R. (1990). Developmental expression of glial fibrillary acidic protein mRNA in the rat brain analyzed by in-situ hybridization. J. Neurosci. Res. *25*, 194–203.

Lazarides, E. (1980). Intermediate filaments as mechanical integrators of cellular space. Nature *283*, 249–256.

McCall, M.A., Gregg, R.G., Behringer, R.R., Brenner, M., Delaney, C.L., Galbreath, E.J., Zhang, C.L., Pearce, R.A., Chiu, S.Y., and Messing, A. (1996). Targeted deletion in astrocyte intermediate filament (Gfap) alters neuronal physiology. Proc. Natl. Acad. Sci. USA *93*, 6361–6366.

McKinnon, R.D., Matsui, T., Dubois-Dalcq, M., and Aaronson, S.A. (1990). FGF modulates the PDGF-driven pathway of oligodendrocyte development. Neuron *5*, 603–614.

Michaelson M.D., Bieri, P.L., Mehler, M.F., Xu, H., Arezzo, J.C., Pollard, J.W., and Kessler, J.A. (1996). CSF-1 deficiency in mice results in abnormal brain development. Development, in press.

Moore, G.R.W., and Raine, C.S. (1988). Immunogold localization and analysis of IgG during immune-mediated demyelination. Lab. Invest. *59*, 641–648.

Moore, G.R.W., McCarron, R.M., McFarlin, D.E., and Raine, C.S. (1987). Chronic relapsing necrotizing encephalomyelitis produced by myelin basic protein in mice. Lab. Invest. *57*, 157–167.

Nicholson, C., and Freeman, J.A. (1975). Theory of current source–density analysis and determination of conductivity tensor for anuran cerebellum. J. Neurophysiol. *38*, 356–368.

Noble, M., Murray, K., Stroobant, P., Waterfield, M.D., and Riddle, P. (1988). Platelet derived growth factor promotes division and motility and inhibits premature differentiation of the oligodendrocyte/type-2 astrocyte progenitor cell. Nature *333*, 560–562.

Pekny, M., Leveen, P., Pekna, M., Eliasson, C., Berthold, C.-H., Westermark, B., and Betsholtz, C. (1995). Mice lacking glial fibrillary acidic protein display astrocytes devoid of intermediate filaments but develop and reproduce normally. EMBO J. *14*, 1590–1598.

Privat, A., Giminez-Ribotta, M., and Ridet, J.-L. (1995). Morphology of astrocytes. In Neuroglia, H. Kettenmann and B.R. Ransom, eds. (New York: Oxford University press), pp. 3–22.

Raff, M.C., Lillien, L.E., Richardson, W.D., Burne, J.F., and Noble, M.D. (1988). Platelet derived growth factor from astrocytes drives the clock that times oligodendrocyte development in culture. Nature *333*, 562–565.

Raine, C.S. (1984). On the association between perinodal astrocytic processes and the node of Ranvier in the central nervous system. J. Neurocytol. *13*, 21–27.

Raine, C.S. (1991). Oligodendrocytes and central nervous system myelin. In Textbook of Neuropathology, second edition, R.L. Davis and D.M. Robertson, eds. (Baltimore, Maryland: Williams and Wilkins), pp. 115–141.

Rakic, P. (1981). Neuronal–glial interactions during brain development. Trends Neurosci. *4*, 184–187.

Richardson, W.D., Pringle, N., Mosley, M.J., Westermark, B., and Dubois-Dalcq, M. (1988). A role for platelet derived growth factor in normal gliogenesis in the central nervous system. Cell *53*, 309–319.

Shibuki, K., Gomi, H., Chen, L., Bao, S., Kim, J.J., Wakatsuki, H., Fujisaki, T., Fujimoto, K., Katoh, A., Ikeda, T., Chen, C., Thompson, R.F., and Itohara, S. (1996). Deficient cerebellar long term depression, impaired eyeblink conditioning, and normal motor coordination in glial fibrillary acidic protein mutant mice. Neuron *16*, 587–599.

Sirotkin, A.M., Edelmann, W., Cheng, G., Klein-Szanto, A., Kucherlapati, R., and Skoultchi, A.I. (1995). Mice develop normally without the H1(0) linker histone. Proc. Natl. Acad. Sci. USA *92*, 6434–6438.

Skoff, R. (1976). Myelin deficit in the jimpy mouse may be due to cellular abnormalities in astroglia. Nature *264*, 560–562.

Vaughn, J.E., and Peters, A. (1967). Electron microscopy of the early postnatal development of fibrous astrocytes. Am. J. Anat. *121*, 131–152.

Virchow, R. (1846). Ueber das granulierte Aussehen der Wandungen der Gehirnventrikel. Allg. Z. Psychiatr. *3*, 242–255.

Weinstein, D.E., Shelanski, M.L., and Liem, R.K.H. (1991). Suppression by antisense mRNA demonstrates a requirement for the glial fibrillary acidic protein in the formation of stable astrocytic processes in response to neurons. J. Cell Biol. *112*, 1205–1213.

Wren, D., and Noble, M. (1989). Oligodendrocytes and oligodendrocyte-type-2 astrocyte progenitor cells of adult rats are specifically susceptible to the lytic effects of complement in absence of antibody. Proc. Natl. Acad. Sci. USA *86*, 9025–9029.

Wu, E., and Raine, C.S. (1992). Multiple sclerosis: interactions between oligodendrocytes and hypertrophic astrocytes and their occurrence in other, nondemyelinating conditions. Lab. Invest. *76*, 88–99.

Yu, A.C.H., Lee, Y.-L., and Eng, L.F. (1991). Inhibition of GFAP synthesis by antisense RNA in astrocytes. J. Neurosci. Res. *30*, 72–79.

Yu, A.C.H., Lee, Y.-L., and Eng, L.F. (1993). Astrogliosis in culture. I. The model and the effect of antisense oligonucleotides on glial fibrillary acidic protein synthesis. J. Neurosci. Res. *34*, 295–303.